Available online at www.sciencedirect.com
ScienceDirect
Journal of Power Sources 162 (2006) 469–473
JOURNAL OF POWER SOURCES
www.elsevier.com/locate/jpowsour

Short communication

Diagnostic tool to detect liquid water removal in the cathode channels of proton exchange membrane fuel cells

H.P. Ma [a,b], H.M. Zhang [a,*], J. Hu [a], Y.H. Cai [a,b], B.L. Yi [a]

[a] *Lab of PEMFC Key Materials and Technologies, Dalian Institute of Chemical Physics, Chinese Academy of Sciences, 457 Zhongshan Road, Dalian 116023, PR China*
[b] *Graduate School of Chinese Academy of Sciences, Beijing 100039, PR China*

Received 7 June 2006; received in revised form 19 June 2006; accepted 19 June 2006
Available online 1 August 2006

Abstract

A transparent PEMFC with a single straight channel was designed to study liquid water transport in the cathode channel. The pressure-drop between the inlet and outlet of the channel was measured and used as a diagnostic signal to monitor liquid water accumulation and removal. This method was non-destructive for the fuel cell, and is capable of monitoring the water droplet buildup and removal in the channel on-line directly, and giving real-time liquid water buildup information. The proper velocity for liquid water removal can be determined according to the pressure-drop curve, which was very helpful to design a flow field and to optimize fuel cell operation. Under the study conditions, and to ensure liquid water discharge, the gas velocity should not lower than 2, 3 and 5 m s^{-1} for 600, 1000 and 1200 mA cm^{-2}, respectively. The results were further verified by visualization in a transparent PEMFC.

Keywords: Transparent PEMFC; Pressure-drop; Flooding; Liquid water removal

1. Introduction

Low emissions, cold start-up capability, high efficiency and the high power density of proton exchange membrane fuel cells (PEMFCs) have made them an attractive power source not only for space and military applications, but also for electric vehicles and mobile devices [1–5]. During operation, the performance of a PEMFC is influenced by many factors. Indeed, water flooding often is the main cause of serious performance drops in PEMFCs [6]. Understanding of the water distribution and removal in PEMFCs is a key to avoid flooding.

Besides modeling [7–10], experiments [11–15] had been carried out to probe the water transport and distribution in an operating PEMFC, including by neutron radiography, nuclear magnetic resonance (NMR) and by gas chromatographic measurements, etc. However, limited by the inherent nature of these technologies, it is hard to investigate the real-time liquid water distribution and removal in PEMFCs [16]. Optical diagnostics [17,18] are non-destructive and capable of monitoring water droplet buildup and removal in the channels directly on-line. Most studies have only focused on the water distribution and reports on the evaluation parameters of liquid water removal in the channels are rare.

In this paper, a transparent PEMFC was designed to study the correlation between liquid water removal and the pressure-drop between the inlets and outlets of the channels (ΔP). Pressure-drop measurements are established as a suitable diagnostic tool to determine the effects of gas velocity on liquid water removal in a straight channel.

2. Experiment

2.1. Design of the transparent PEMFC

The structure of the transparent fuel cell is shown as Fig. 1.

Flow field plates were made with graphite, which also acted as current collectors. In the cathode, a single straight channel was adopted. The channel width was 1.5 mm, depth 1 mm and length 125 mm. On the backside of anode flow field plate, water

* Corresponding author. Tel.: +86 411 84379072; fax: +86 411 84665057.
E-mail address: zhanghm@dicp.ac.cn (H.M. Zhang).

0378-7753/$ – see front matter © 2006 Elsevier B.V. All rights reserved.
doi:10.1016/j.jpowsour.2006.06.055

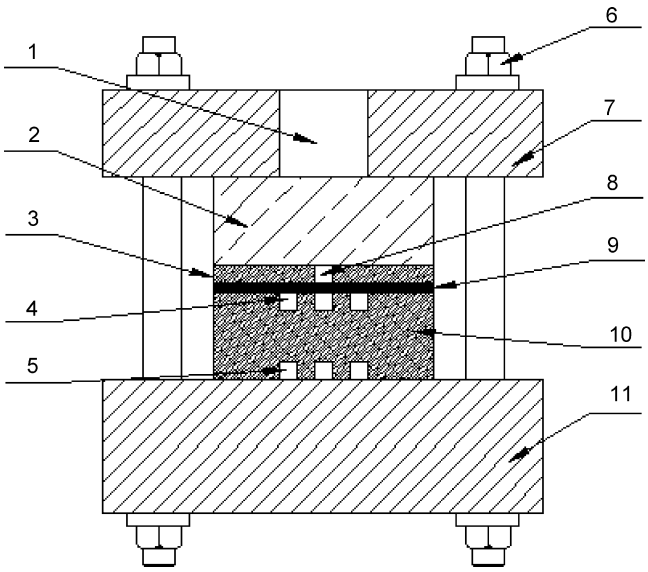

Fig. 1. Schematic of the transparent fuel cell: (1) window; (2) transparent cover plate; (3) cathode flow field plate; (4) anode channel; (5) recycled water channel; (6) bolt; (7) cathode clamp; (8) cathode channel; (9) MEA; (10) anode flow field plate; (11) anode endplate.

channels were carved, through which recycled water passed to maintain the cell temperature.

The membrane electrode assemblies (MEAs) used in this study were made in our laboratory, using JM 40% Pt/C catalyst, Toray wet-proof carbon paper for the GDL backing layers, and Nafion 1035 membrane. Electrodes were prepared by scraping catalyst ink (Pt/C catalyst mixed with PTFE solution) onto the backing layer. The active area of the MEA was 5 cm^2 (4× 125 mm) and catalyst loadings on both electrodes were about 0.5 Pt mg cm^{-2}.

2.2. Experimental set-up

The experimental set-up is shown in Fig. 2. It consists of a gas supply unit, the fuel cell system, a digital camera, an electric load and a computer for data acquisition.

Pure hydrogen and oxygen gas were used. Before entering into the fuel cell, reactants were humidified by the bubbler-type humidifier. To avoid water condensation, pipelines between the humidifier and the cell were wrapped with heating tapes. The cell temperature was maintained through recycled water, which was supplied by a thermostat water bath. The pressure-drop between the inlet and outlet of the cathode was monitored with differential manometer (Honeywell S900). The operational current, voltage and pressure-drop were recorded by the data acquisition system. Photos of the cathode channel were taken every 5 s by digital camera (DIMAGE-A2). Before each experiment, a nitrogen purge process was used to clean out the residual fuel and oxidant in the cell and pipelines.

The transparent PEMFC was posited upright. The anode humidification temperature and cell temperature were 60 °C. The pressures in the anode and cathode were 0.1 MPa. The flow rate of hydrogen was 87 ml min^{-1}. The operational current density (I), cathode humidification temperature (T_{hc}) and oxygen

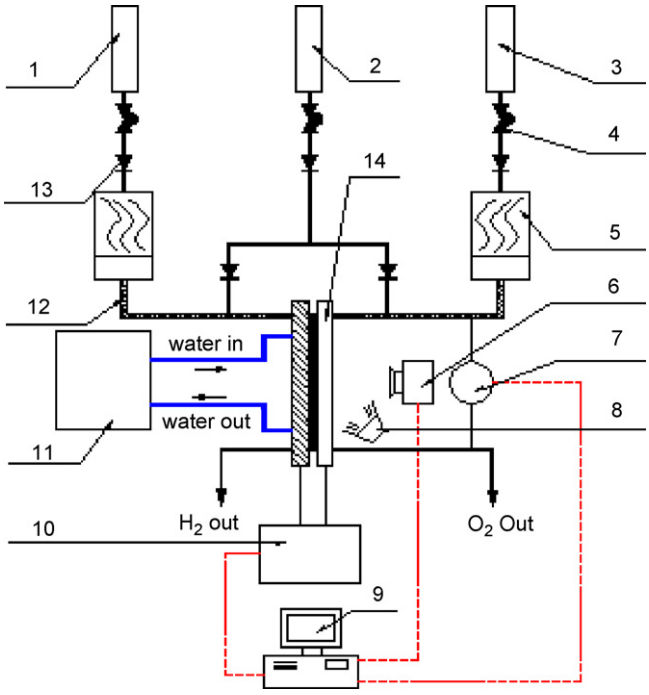

Fig. 2. Experiment set-up: (1) hydrogen tank; (2) nitrogen tank; (3) oxygen tank; (4) pressure maintaining valve; (5) humidifier; (6) digital camera; (7) differential manometer; (8) light source; (9) data collector system; (10) electronic load; (11) thermostat water bath; (12) heating tape; (13) one-way valve; (14) the transparent fuel cell.

velocity in the channel (μ_{O_2}) were given later for each experimental case study.

3. Results and discussion

3.1. Correlation between the pressure-drop and liquid water removal in the straight channel

In this experiment, I was 1000 mA cm^{-2}, T_{hc} was 40 °C, and u_{O_2} was 1.5 m s^{-1}.

Fig. 3 shows the photos taken at 320, 325, 370, 375, 635 and 640 s. Fig. 4 shows ΔP between 0 and 700 s.

At 0 s there was no liquid water in the channel, and ΔP was the lowest. At 70 s, the first water droplet emerged, which was stressed by three forces: gravitation (G), viscous force between droplet and solid surface (F_s), and shear drag force induced by the gas flow (F_D), as seen in Fig. 5. G and F_s are proportional to

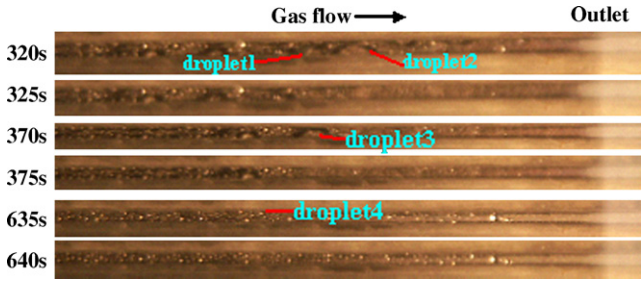

Fig. 3. Photos taken at 285, 290, 320, 325, 635 and 640 s. T_{hc} = 40 °C, u_{O_2} = 1.5 m s^{-1}, I = 1000 mA cm^{-2}.

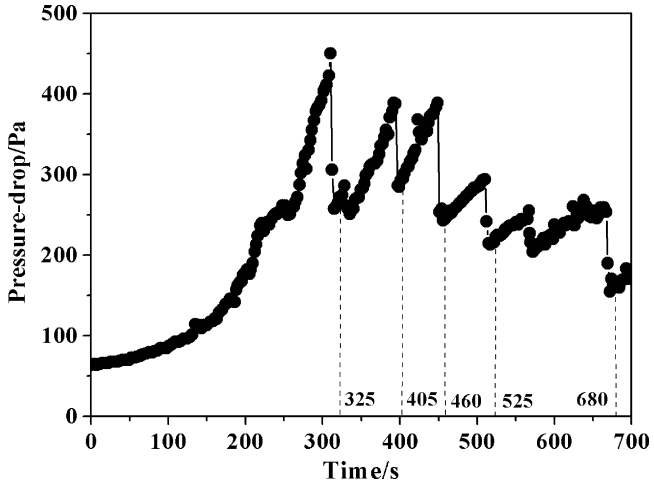

Fig. 4. Pressure-drop between 0 and 700 s. $T_{hc} = 40\,^{\circ}C$, $u_{O_2} = 1.5\,m\,s^{-1}$, $I = 1000\,mA\,cm^{-2}$.

the droplet volume and the contact area between the droplet and solid surface respectively. And F_D increases with the increase of gas velocity and projected area of the droplet normal to the flow direction.

The droplet was small at the beginning, $F_D + G \leq F_s$, and was held on the GDL surface or/and the channel sidewall. With continued operation of the fuel cell, more droplets emerged and grew larger, which hindered the gas flow and led to an increase of ΔP. At 320 s, droplet 1 grew to a critical size, $F_D + G = F_s$. At 325 s droplet 1 moved towards the outlet and merged with the big droplet 2. Then a bigger droplet emerged and blocked the channel. After that, all the water drops between droplet 1 and the outlet were blown out. The channel was unobstructed and ΔP declined from a peak value 450–257 Pa sharply. At 375 s, because there was no other droplet between droplet 3 and the outlet, only droplet 3 was discharged. The water removal did not block the channel and had little effect on the ΔP. At 640 s, droplet 4 on GDL was removed. It was so small that the water removal hardly had any influence on ΔP. Because the GDL is hydrophobic, F_s decreases greatly and the droplets with small size can be removed. In addition, model [19] also revealed that a hydrophobic surface was beneficial to droplet removal.

It was noted that blocking discharge resulted from the large accumulation of liquid water on the surface of the MEA and the channel sidewall. The liquid water on the MEA would hinder the transportation of reactant to the reaction site, and influence the cell performance greatly. So the ideal mode was that water drops were discharged in time.

From 0 to 700 s, five incidents of ΔP sharp decline and five incidents of blocking were observed in the transparent fuel cell. Each blocking discharge time is marked in Fig. 4. It shows that the ΔP sharp decline directly corresponded with the blockage discharging.

From the foregoing analysis, ΔP increased with the increase of liquid water content in the channel and the ΔP sharp decline corresponded to discharge of the blockage. That is, ΔP could be used as an obvious signal of liquid water accumulation in the channel [20]. It could be used to determine the mode of droplet discharged during fuel cell operation. If the curve of ΔP had large fluctuations, this reveals that liquid water did not discharge regularly.

3.2. Effect of gas velocity on liquid water removal in the straight channel

In the experiments, T_{hc} was 60 °C, I was 1000 mA cm^{-2} and u_{O_2} was set at 1.0, 2.0 and 3.0 m s^{-1}, respectively. Fig. 6 shows the ΔP between 0 and 1800 s with different velocities.

At the beginning of the operation, there was no liquid water in the GDL and the channel. Product water could be expelled from the GDL quickly and ΔP increased rapidly. For each velocity, almost in the same time, ΔP reached a peak value.

After 1000 s, the fuel cell reached steady state. At 1 m s^{-1}, ΔP fluctuated frequently with large amplitudes. This reveals

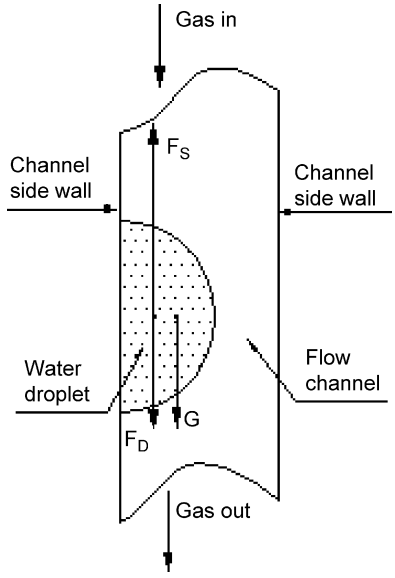

Fig. 5. Force diagram of water droplet in the channel.

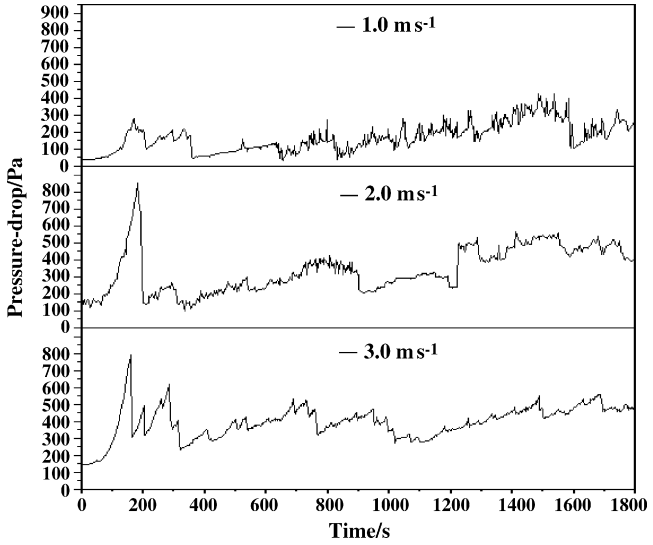

Fig. 6. Pressure-drop between 0 and 1800 s with velocity of 1, 2 and 3 m s^{-1}. $T_{hc} = 60\,^{\circ}C$, $I = 1000\,mA\,cm^{-2}$.

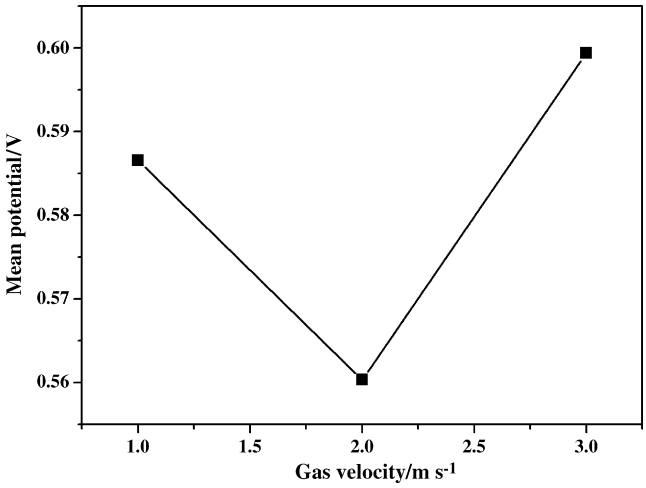

Fig. 7. Mean potential between 1000 and 1800 s with velocity of 1, 2 and 3 m s^{-1}. T_{hc} = 60 °C, I = 1000 mA cm^{-2}.

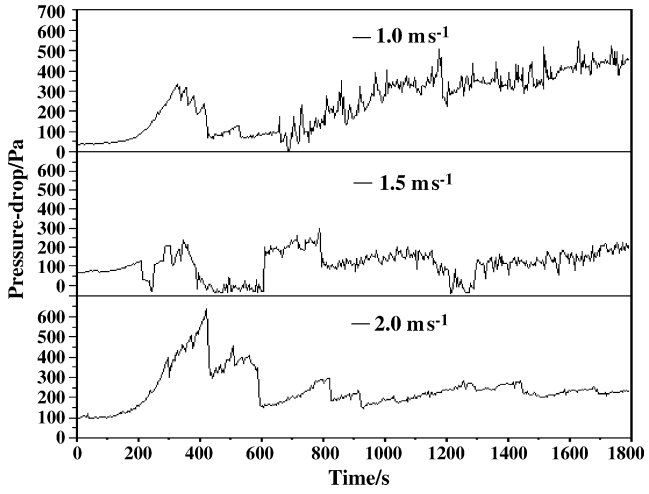

Fig. 8. Pressure-drop between 0 and 1800 s with velocity of 1, 1.5 and 3 m s^{-1}. T_{hc} = 60 °C, I = 600 mA cm^{-2}.

that discharge of the blockage is the major mode of liquid water removal. At 2 m s^{-1}, the frequency of ΔP sharply declined, but there also were large fluctuations of ΔP. At 3 m s^{-1}, the ΔP curve became smooth. This means that liquid water is discharged in time. Visualization of the transparent fuel cell also indicated that there were few channels blocked and little liquid water accumulated in the channels.

Because droplets were influenced by G, F_s and F_D (seen as Fig. 5). F_D increased with the increase of velocity, while G and F_s were maintained as constants. The droplet critical size decreased with increase in velocity. At 1 m s^{-1}, the critical size was large. Droplets often blocked the channel and liquid water was removed by blockage discharge. At 2 m s^{-1}, the critical size was comparable to the channel size, droplets often contacted with the hydrophilic sidewall and spread into a water film [19,21] (the detailed correlation between the droplet critical diameter, channel size and liquid water removal will be discussed in a future article). So most liquid water accumulated in the channel, and the large fluctuation times decreased greatly. At 3 m s^{-1}, the critical size was small, and droplets on GDL could be blown out in time, which was the ideal mode of liquid water removal. Fig. 7 shows the mean potential between 1000 and 1800 s with different velocities. The results also agreed with the analysis. At 2 m s^{-1}, liquid water accumulation was the greatest and the potential was the lowest. At 3 m s^{-1}, water drops were discharged in time—there was little liquid water accumulation and the performance was the highest.

Fig. 8 shows the ΔP of I = 600 mA cm^{-2} with u_{O_2} of 1, 1.5 and 2 m s^{-1}. And Fig. 9 shows the ΔP of I = 1200 mA cm^{-2} with u_{O_2} of 3, 4 and 5 m s^{-1}. For each current density, at low velocity, ΔP fluctuated frequently. With increase of velocity, the ΔP curve became smooth. Tables 1 and 2 give the times of the ΔP sharp declines (>60 Pa) in 1000–1800 s with 600 and 1200 mA cm^{-2}, respectively. This reveals that channel blockage times decreased with increase of velocity. For 600 mA cm^{-2}, the channel was hardly blocked with 2 m s^{-1}. The corresponding velocity with 1200 mA cm^{-2} was 5 m s^{-1}. Photos taken at 1800 s in Fig. 10 show that the droplets were

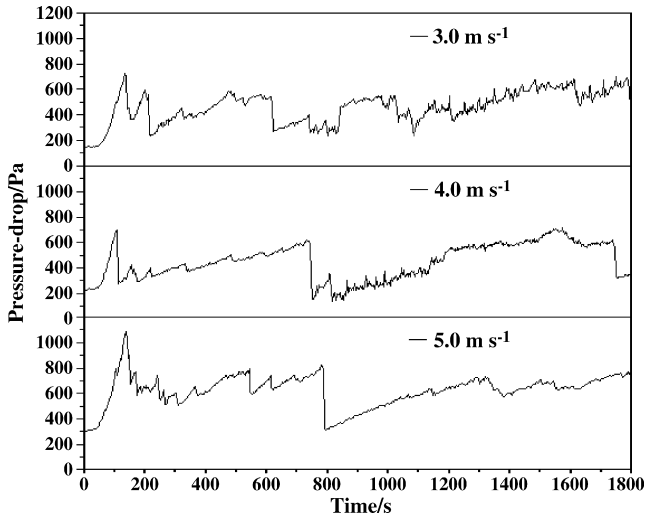

Fig. 9. Pressure-drop between 0 and 1800 s with velocity of 3, 4 and 5 m s^{-1}. T_{hc} = 60 °C, I = 1200 mA cm^{-2}.

Table 1
Times of pressure-drop sharp declines (>60 Pa) with different velocities during 1000–1800 s

Gas velocity (m s^{-1})	Times of ΔP sharp decline
1.0	19
1.5	8
2.0	0

I = 600 mA cm^{-2}.

Table 2
Times of pressure-drop sharp declines (>60 Pa) with different velocities during 1000–1800 s

Gas velocity (m s^{-1})	Times of ΔP sharp decline
3.0	16
4.5	2
5.0	0

I = 1200 mA cm^{-2}.

Fig. 10. Photos taken at 1800 s: (1) $I = 600\,\mathrm{mA\,cm^{-2}}$ and $u_{O_2} = 2\,\mathrm{m\,s^{-1}}$ and (2) $I = 1200\,\mathrm{mA\,cm^{-2}}$ and $u_{O_2} = 5\,\mathrm{m\,s^{-1}}$.

small, and there was almost not liquid water accumulation in the channel. The ΔP curve could be used to determine the most suitable gas velocity for liquid water removal. This would help with the flow field design and the selection of fuel cell operation conditions.

4. Conclusions

The pressure-drop between the inlet and outlet of the channel (ΔP) was monitored during fuel cell operation and ΔP was recorded. A transparent PEMFC with a single straight channel for the cathode was designed to investigate the correlation between ΔP and liquid water removal. ΔP increased with the increase of liquid water content in the channel and a ΔP sharp decline corresponded to discharge of a water blockage. ΔP thus could be used as a diagnostic signal to monitor liquid water accumulation and removal in the channel.

5. Summary

(1) The diagnostic tool could be used as a non-destructive tool to give real-time liquid water information in the cathode channel during operation. According to the ΔP curve, it is easy to determine the best velocity for liquid water removal. This is of great benefit to the design of the flow field and the optimization of the fuel cell operation conditions.
(2) To ensure liquid water removal, the gas velocity should not be lower than 2, 3 and $5\,\mathrm{m\,s^{-1}}$ for 600, 1000 and $1200\,\mathrm{mA\,cm^{-2}}$, respectively.

Acknowledgments

The authors gratefully acknowledge the financial support from the National Natural Science Key Foundation of China (No. 50236010) and the State Key Development Program for Basic Research of China (No. G2000026410).

References

[1] J. Tatiana, P. Freire, E.R. Gonzalez, J. Electroanal. Chem. 503 (2001) 57–68.
[2] V. Mehta, J.S. Cooper, J. Power Sources 114 (2003) 32–53.
[3] S.G. Chalk, J.A. Milliken, J.F. Miller, J. Power Sources 71 (1998) 26–35.
[4] K.H. Choi, D.H. Peck, C.S. Kim, D.R. Shin, T.H. Lee, J. Power Sources 86 (2000) 197–201.
[5] I. Bar-On, R. Kirchain, R. Roth, J. Power Sources 109 (2002) 71–75.
[6] J.J. Baschuk, X. Liu, J. Power Sources 86 (2000) 181–196.
[7] P. Quan, B. Zhou, A. Sobiesiak, Z. Liu, J. Power Sources 152 (2005) 131–145.
[8] K. Jiao, B. Zhou, P. Quan, J. Power Sources 154 (2006) 124–137.
[9] A. Golpaygan, N. Ashgriz, Int. J. Energy Res. 29 (2005) 1027–1040.
[10] U. Pasaogullari, C.Y. Wang, J. Electrochem. Soc. 151 (2004) A399–A406.
[11] A.B. Geiger, A. Tsukada, E. Lehmann, P. Vontobel, A. Wokaun, G.G. Scheree, Fuel Cells 2 (92) (2002) 92–98.
[12] R. Satija, D.L. Jacobson, M. Arif, S.A. Werner, J. Power Sources 129 (2004) 238–245.
[13] K.W. Feindel, L.P.-A. LaRocque, D. Starke, S.H. Bergens, R.E. Wasylishen, J. Am. Chem. Soc. 126 (2004) 11436–11437.
[14] S. Tsushima, K. Teranishi, S. Hirai, Energy 30 (2005) 235–245.
[15] M.M. Mench, Q.L. Dong, C.Y. Wang, J. Power Sources 124 (2003) 90–98.
[16] X.G. Yang, F.Y. Zhang, A.L. Lubawy, C.Y. Wang, Electrochem. Solid-State Lett. 7 (2004) A408–A411.
[17] K. Tüber, D. Pócza, C. Hebling, J. Power Sources 124 (2003) 403–414.
[18] A. Hakenjos, H. Muenter, U. Wittstadt, C. Hebling, J. Power Sources 131 (2004) 213–216.
[19] Y.H. Cai, J. Hu, H.P. Ma, B.L. Yi, H.M. Zhang, J. Power Sources 161 (2006) 843–848.
[20] F. Barbir, H. Gorgun, X. Wang, J. Power Sources 141 (2005) 96–101.
[21] F.Y. Zhang, X.G. Yang, C.Y. Wang, Electrochem. Solid-State Lett. 2 (2006) A225–A232.